Applied Thermal Engineering 257 (2024) 124294

Contents lists available at ScienceDirect

Applied Thermal Engineering

journal homepage: www.elsevier.com/locate/apthermeng

Research Paper

Experimental study of the optimal design and performance of a mixed-flow dew-point indirect evaporative cooler

Alessandra Urso [a,b], Eloy Velasco-Gómez [b], Ana Tejero-González [b,*], Manuel Andrés-Chicote [b], Francesco Nocera [a]

[a] Department of Civil Engineering and Architecture (DICAR), University of Catania, 95125 Catania, Italy
[b] Departamento de Ingeniería Energética y Fluidomecánica, Grupo de Investigación de Termotecnia, Instituto de las Tecnologías Avanzadas de la Producción (ITAP), Escuela de Ingenierías Industriales, Universidad de Valladolid, Paseo del Cauce No. 59, 47011 Valladolid, Spain

ARTICLE INFO

Keywords:
Cooling energy poverty
Experimental study
Dew point indirect evaporative cooler
Mixed-flow configuration
Polycarbonate plates

ABSTRACT

Evaporative cooling technologies represent a promising alternative to face the emerging cooling energy poverty, owing to their low production and operative costs. High performance can be achieved through more complex designs, such as dew point indirect evaporative cooling (DIEC) systems. Recent literature explores improvements on these systems, like flow configuration, materials, and water distribution. This study proposes a compact mixed-flow DIEC system made of polycarbonate plates covered with two possible wicking materials. Three water distribution systems are also studied. The prototypes are experimentally characterised by varying the inlet air temperature, humidity, volume flow, and working-to-intake air ratio. The best performing design is evaluated in terms of temperature drop, dew-point effectiveness, wet-bulb effectiveness, and cooling capacity. Results are consistent with those in the literature for equivalent heat transfer areas. The use of a wicking material improves the cooling capacity by up to 1.45. The type of material is less relevant, which enables to select the most economic and accessible option. External nozzles for water distribution offers temperature drops of more than 1 °C and better cooling capacities of approximately 100 W than inlet water distributors.

1. Introduction

Energy poverty is an emerging topic in the European Union, especially after the Covid-19 pandemic and the energy crisis due to the war in Ukraine [1]. It could be defined as the incapability of a householder to avail adequate domestic energy services, namely space heating, cooling, or cooking [2].

In particular, the problem of cooling energy poverty is still not well-explored in European scientific literature [2], even if it has been gaining more attention amid the rising temperatures due to global warming and the consequent increase in energy demand for indoor space cooling. As reported in [3], the increase in cooling demand may force the lowest income households into summer energy poverty. This problem may become more evident in southern European countries, such as Greece, Italy, and Spain, which are more vulnerable to high temperatures and heatwaves [3].

Among the existing alternative cooling systems to mechanical vapor compression, evaporative coolers (ECs) are drawing interest in recent years for their higher coefficient of performance (COP) [4] and the possibility of low production costs [5,6]. In addition, ECs have a simple and compact design, i.e., they can be installed in buildings easily [7]. Despite these undisputable advantages, ECs do not outperform in the market [5].

The main drawback of the ECs is that their effectiveness is strongly dependent on the humidity levels in the air supply, which is drawn from the outside. Therefore, they find applicability only in the hot-and-dry climate. By considering the European Köppen–Geiger map, hot and dry summer seasons are characteristic of the Mediterranean coast, and they are expected to be dominant in the rest of southern Europe in future decades [8]. Moreover, recent studies have attempted to integrate dehumidification methods with ECs, which extends the application of ECs to temperate and humid areas [6]. Therefore, the limited climate applicability of evaporative coolers cannot justify their scarce diffusion in the present and future European markets.

Despite the scientific advancement of this technology, persistent challenges, e.g., water consumption and complexity of equipment, especially those of water distributors [5], should be solved to commercialize these systems.

* Corresponding author.
E-mail address: ana.tejero@uva.es (A. Tejero-González).

https://doi.org/10.1016/j.applthermaleng.2024.124294
Received 29 April 2024; Received in revised form 6 August 2024; Accepted 29 August 2024
Available online 7 September 2024

Nomenclature

Acronyms and abbreviations

EC	Evaporative cooler
COP	Coefficient of performance
DEC	Direct evaporative cooler
HMX	Heat and mass exchange
IEC	Indirect evaporative cooler
DPIEC	Dew-point indirect evaporative cooler
AHU	Air handling unit
OP-in	Orifice plate in the inlet channel
OP-out	Orifice plate in the outlet channel
TH-in	Temperature and relative humidity sensor in the inlet air entrance
TH1-out	Temperature and relative humidity sensor in the primary air exit
TH2-out	Temperature and relative humidity sensor in the secondary air exit
Tw	Temperature sensor in the water tank
CoF	counter-flow
CrF	cross-flow

Symbols

L_d	Dry channel length (cm)
W_d	Dry channel width (mm)
H_d	Dry channel height (mm)
L_w	Wet channel length (cm)
W_w	Wet channel width (cm)
G_w	Wet channel gap (mm)
$\dot{m}$	Mass flow (kg/h)
R	Working-to-intake air ratio
T	Temperature (°C)
RH	Relative humidity (%)
$\dot{V}$	air volume flow (m^3/s)
K	Characteristic of OP
Δp	Pressure drop (Pa)
v	Specific volume (m^3/kg)
ε	Effectiveness
$\dot{q}$	Cooling capacity (W)
A	Area (m^2)
V	velocity (m/s)

Subscripts

tot	Total air
pr	Primary air
sec	Secondary air
wb	Wet bulb
dp	Dew point
w	Water
HT	Heat transfer

1.1. Evaporative cooling technologies and working principles

ECs leverage the effect of water evaporation to cool down the ambient air: when air interacts with water, the sensible heat in the air is converted to latent heat by an isenthalpic process. Based on the interaction between the supply air (i.e., the air to be introduced into the indoor space) and water, ECs are classified into direct evaporative coolers (DEC) and indirect evaporative coolers (IEC) [9].

In DEC, the supply air comes in direct contact with water. This system provides a higher temperature drop, but inevitably increases the moisture content in the supply air. In some cases, this renders the system less effective in guaranteeing adequate hygrothermal comfort in occupied spaces [10]. Conversely, in IEC, humidification of the supply (or primary) air is avoided by combining the evaporative cooling process in a working (or secondary) airstream with a heat exchanger [11].

To improve the performance of IEC and overcome the limitations of DEC, a study proposed the dew-point indirect evaporative cooler (DPIEC) [12]. A DPIEC is an IEC in which part of the supply air in the dry channel is diverted to the wet channel as the working fluid. Thus, the working fluid is pre-cooled and to a temperature below its wet-bulb temperature. This temperature eventually reaches the dew-point temperature as the process is repeated cyclically. The Maisotsenko cycle maximizes this potential, and its application is now prevalent in various fields [13].

DPIECs offer a higher temperature drop than conventional ECs, as well as higher cooling capacity, provided the ratio between secondary and intake air is properly dimensioned. This has the advantage of an improved COP, reduced energy consumption, compactness for easy installation in buildings [14], raw material conservation, and reduced miscellaneous costs.

1.2. Improved designs of DPIEC systems

Despite the high energy efficiency and low environmental impact of DPIEC systems, several issues related to their design, such as optimal water supply, promotion of auto-wicking, and selection of durable materials with the best thermal transfer properties and water retention [12], must be addressed. Various studies have focused on the effects of flow configuration, material, and water supply system.

1.2.1. Flow configuration

The flow configuration refers to the direction of primary air flow relative to the secondary air flow. Typically, DPIEC systems are designed in the counter-flow or cross-flow configuration. In counter-flow, the primary air flows in the opposite direction of the secondary air, whereas in cross-flow, the primary air flows in the transverse direction of the secondary air. Counter-flow DPIEC systems have demonstrated better cooling effectiveness and capacity than the cross-flow DPIEC [14], despite larger pressure drops. However, this comes at the cost of higher electrical power consumption [15]. Sohani et al. [16] found out that the counter-flow configuration performed better in arid areas, while in other climates the cross-flow configuration was the better alternative. On contrary, [17] obtained higher exergy efficiency for the cross-flow configuration, in addition to less water consumption, with comparable electricity consumption and carbon emissions than the counter-flow configuration. In addition, as reported in [18], the cross-flow configuration can potentially save more installation space. Moreover, efforts to fabricate and commercialize counter-flow DPIECs have encountered several difficulties at the early design phase [15]. This demonstrates that cross-flow DPIECs are more preferred in the market. Additionally, the complex design of the counter-cross configuration may disturb the air distribution, as per a numerical analysis by [19]. In fact, it revealed that a non-uniform air distribution in complex geometries reduced the efficiency of air cooling.

As an alternative, [20] proposed a counter–cross-flow DPIEC that consists of both counter- and cross-flow channels. On the one hand, the performance of this device is comparable to that of the counter-flow DPIEC, with the advantage of reduced volume and weight of the cooler, while providing the same air volume. Other alternative configurations were proposed by [21–23]. In particular, [22] tested a mixed-flow DPIEC in which the secondary air flowed into a plate without a constrained direction. They found that this configuration ensured better

cooling performance and effectiveness than the conventional ones. Although this device is expected to be facile and inexpensive to produce owing to its simpler design, the study did not analyse the compactness, cost, or water consumption of the system.

1.2.2. Materials

The material selected that can facilitate high heat transfer between wet and dry channels, as well as an even distribution and storage of water on the wet side [24]. Regarding the thermal conductivity of the plates, thicknesses below 0.25 mm would result in a low thermal resistance irrespective of the thermal properties of the material [25]. Moreover, the use of high-porosity materials that absorb and store water inside the pores would improve the saturation of the working fluid (air) throughout the wet channels. However, humidification of the dry channels must be avoided.

The strategy adopted in recent studies [22,24,26–28] involved selection of the plate material and a wicking material to cover the surface of the wet channels. The plate material forms the rigid, low-thermal-resistance, and impermeable heat exchanger. With this aim, Al, polyvinyl chloride (PVC), and polypropylene (PP) are commonly used as the plate material. Meanwhile, the function of the wicking material is to absorb and retain water, while also possessing a low thermal resistance. Fibrous materials are commonly used as wicking materials [29]. Among them, cloth fabrics are widely preferred for their availability, durability, and pliability. Moreover, they should induce lower thermal resistance and pressure drop [7].

Reference [27] used a PP plate coated with nylon fabric on the wet side. Similarly, [22] used Al coated with cotton. Instead, [26] used PVC sheets coated with an unspecified hydrophilic material. Reference [24] experimentally tested several fibrous materials: flocking fibres, Coolplus fibre, Spunlace nonwoven fabrics, and Kraft paper. Ultimately, they chose Coolplus fibre to coat the Al channel walls.

As an alternative, the fibrous materials can be used to form a composite membrane material along with a hydrophobic material on the side of the dry channel [29]. For example, [30] used a polymer–plant-fibre composite material and a plastic bracket.

Notably, the performance of the material used in DPIEC is tested to determine the water absorption and retention [29], which might influence the saturation rate of the secondary air. However, the literature contains few studies that have compared the performances of different materials by applying them to DPIEC. For example, [20] compared a prototype made of Al with the same prototype made of polystyrene covered with nylon. The performance of the DPIEC was evaluated in terms of temperature drop and dew-point effectiveness.

In addition, other aspects should be considered in the selection of channel materials, e.g., durability, workability, availability, last, and costs.

1.2.3. Water supply system

The water supply system must uniformly distribute the water droplets through the wicking material to enhance the saturation of secondary air and reduce heat transfer resistance between the wet and dry paths [31]. It must also minimize the water and electric consumptions, as well as allow free passage of air throughout the channels.

The most used water-supply system in DPIECs consists of a water spray installed at the top of the wet side. However, this type of system exhibits the disadvantages of large water consumption, water droplet drift, and non-uniform water distribution [24]. To overcome these challenges, studies on IECs, such as [32] and [33], focused on optimizing the nozzle configuration. In particular, [32] experimentally tested and compared five commonly used spray nozzles (spiral, conical, square, sector type, target impact) and found out that the spiral type enhanced the uniformity of distribution the most. Additionally, they proposed an intermittent spray to save water and energy consumption. Reference [33] proposed and experimentally validated a three-dimensional spray model based on computational fluid dynamics. Thus, they designed an optimal configuration based on the droplet diameter (0.25 mm), pressure (1.5 bar), flowrate (5.4 l/min), spray cone angle (68°) and distance between nozzles (80 mm). The study found out that the optimized solution could increase the wet-bulb efficiency and COP by 15.1 % and 17.6 %, respectively. A recent study on IEC by [34] proposed intermittent spraying instead of continuous spraying. Although the performance decreased, a noticeable reduction in energy consumption was observed.

To improve the water distribution in DPIECs, [35] constructed a water distributor composed of a series of small tubes drilled and inserted inside the wet channel. Along with the choice of a water-holding material, this device adopted an intermittent water-supply scheme to minimize the water usage and water pump-power consumption. However, this system was expected to induce problems such as a large pressure drop and channel blockage [24]. Alternatively, [24] leveraged the capillary action of wet materials to design an automatic wicking DPIEC. This system was composed of a parallel dry channel and wet channel placed vertically and a water channel installed at the bottom of the wet channel, coated with a wet material. Thus, water was wicked automatically by the wet material through capillary action by forming a stable water film in the wet channel.

Reference [36] studied the optimal configuration between the water supply and the working fluid (air) flow. They observed that higher evaporation was achieved when the air flowed to the water distribution in a crossflow manner. Moreover, [37] numerically evaluated the performance of a DPIEC by changing the supplied fluid to the wet channel. They determined that using a hybrid nanofluid instead of water provided a significant improvement in combination with surface modification, but it was not very fruitful in the case of flat channels.

1.3. Originality and scope of the article

The literature reveals that more complex and high-performance designs of DPIEC systems in aspects including flow configuration, channel materials, and water-supply system have been investigated in recent years.

Regarding flow configuration, the counter-flow configuration performs the best, despite being more complex in construction than the cross-flow configuration. A mixed configuration was proposed to balance effectiveness and ease of design. However, it was not compact. This study proposed a compact mixed-flow configuration and compared its performance with those of the current mixed-flow design.

Regarding material selection, the prototype of the proposed system has a design similar to the existing one: the use of plate materials covered with a wicking material on the wet side. However, unlike with the previous design, we use polycarbonate as the plate material. Two wicking options were studied through direct comparison of their effects on the prototype's performance. Notably, published works on the wicking materials did not study their performance directly on a tested prototype.

Finally, concurring with existing knowledge, uniform water distribution is chosen. While most studies analysed different spray devices, a few also proposed direct supply of water into the wet channels through small pipes. This study compared the performances of the prototype with three different water distributors: two spray-type distributors, one placed outside and the other inside the wet channels, and an inside pipe-ending distributor.

The experiments were carried out by varying the inlet air temperature, humidity, volume flow, and working-to-intake air ratio. The performance of the proposed DPIEC was evaluated in terms of temperature drop, dew-point effectiveness, wet-bulb effectiveness, and cooling

capacity. The results were validated against data from published work.

2. Methodology

2.1. Prototype design and construction

In this study, a novel DPIEC is developed and experimentally tested. The device is composed of overlapping modular elements made of polycarbonate (Fig. 1).

The base element consisted of dry channels and a wet plate, with the latter covered with a wicking material on one side. At the end of the dry channels, a few air paths were blocked and holes were drilled to drive the primary air through the wet channels, forming the secondary air stream. Next, the secondary air stream was vented through the top opening of the device (Fig. 2). As the air stream through the wet channels moves in a hybrid counter–cross-flow configuration, the device is more appropriately defined as a mixed-flow-configuration DPIEC.

A water distributor was installed at the top of the device to supply water to the wet channels.

Fig. 3 illustrates a photograph of the assembled device, along with the inlet and outlet of the air flow.

The device is tested without a wicking material and for two different cloth materials: synthetic and cotton fabrics, as shown in Fig. 4.

Moreover, different types of water distributors were tested (Fig. 5). Distributors 1 and 2 consisted of a circular pipe with additional shorter pipes that penetrated the wet channels. Distributor 1 distributed water simply under the influence of gravity, while Distributor 2 had small nozzles at the end of the pipes to spray water and distribute water more uniformly through the wet channels. Distributor 3 consisted of a circular pipe equipped with nozzles that uniformly spray water over the top of the wet channels. Videos of the operation of the three distributors are provided as supplementary material with this manuscript.

The structural parameters of the device are summarized in Table 1.

2.2. Experimental set up

The test bench is composed of an air handling unit (AHU), a water tank, a water pump, connection ducts, orifice plates for airflow measurement (OP-in and OP-out), and temperature and relative humidity sensors (TH-in, TH1-out, TH2-out, Tw), as displayed in Fig. 6.

A water tank was placed below the prototype, and a submergible pump guaranteed the circulation of water till the water distributor. The power consumption of the pump ranged from 10–20 W with a maximum flow rate of 16 l/min.

Moreover, the prototype was connected to the AHU via flexible air ducts with a diameter of 25 cm. An additional duct with the same characteristics transported the supply air from the prototype to the laboratory. The working air ratio of the secondary air to the primary air flow was controlled with a dumper placed at the exit of the primary airstream duct.

First, the air exhausted from the laboratory was treated in the AHU to reach the required test conditions. Subsequently, it was transported to the prototype. In the dry channels, a fraction of the primary air treated in the prototype was diverted into the wet channels to act as the working (secondary) air. The fraction of the unused treated (primary) air was then pumped to the target indoor space.

During the test, the following factors were monitored:

- total, primary, and secondary air flow rates $\dot{m}_{tot}$, $\dot{m}_{pr}$, and $\dot{m}_{sec}$;
- total, primary, and secondary air temperatures T_{tot}, T_{pr}, and T_{sec};
- total, primary, and secondary air relative humidity RH_{tot}, RH_{pr}, and RH_{sec};
- water temperature T_w.

The air mass flow rate is determined indirectly through the pressure drop measured at the previously calibrated orifice plates, while the other measurements (air dry-bulb temperature, air relative humidity, and water temperature) were measured with the previously calibrated sensors described in Table 2.

To ensure steady-state conditions, all measurements were taken after at least 20 min of operation the experimental set up.

To measure the inlet and outlet primary air flow characteristics, two orifice plates were placed between the AHU and the device (OP-in in Fig. 6) and between the device and the supply duct (OP-out in Fig. 6), respectively.

The orifice plate allows for calculating the air volumetric flow rate $\dot{V}$ by measuring the pressure difference Δp upstream and downstream of the plate (Equation 1).

$$\dot{V} = k \bullet \sqrt{\Delta P} \tag{1}$$

The values of coefficient k in (Equation 1) is a characteristic specific to the orifice plate.

Δp was measured by datalogger Testo 435–4 as the mean value of the instant values of static pressure after 30 s.

The measurement was conducted after a period of at least 20 min

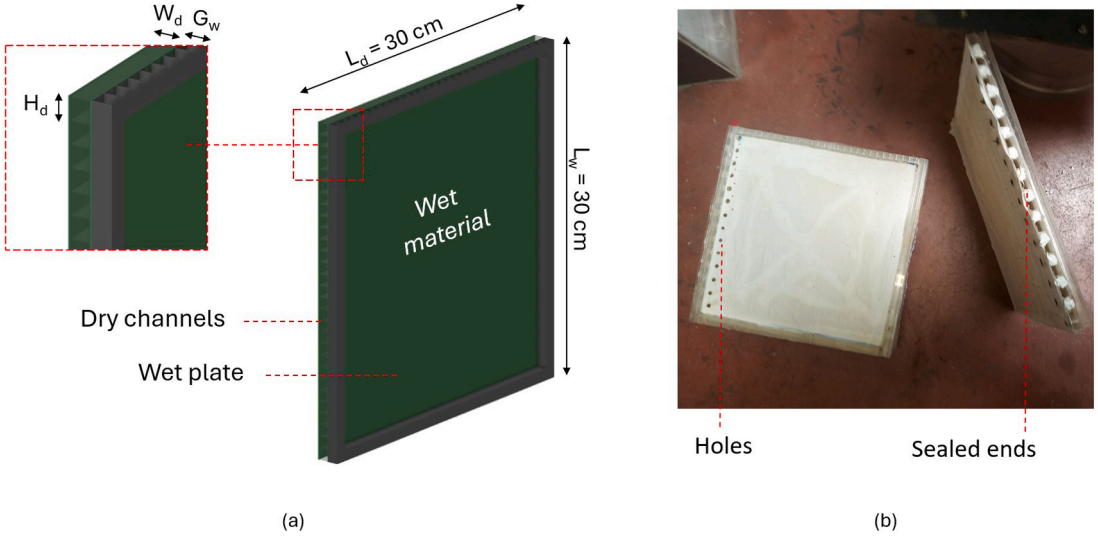

Fig. 1. Three-dimensional (3D) view (a) and photographs (b) of the base element.

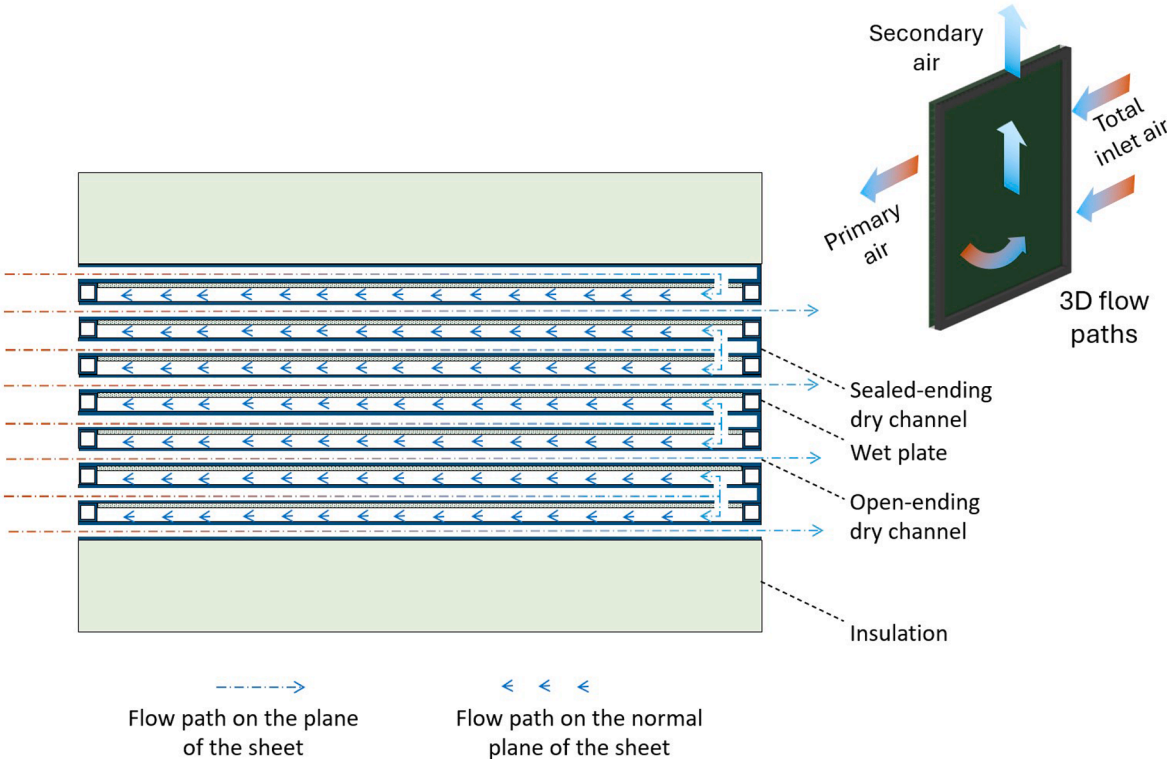

Fig. 2. Schematic section of the prototype and 3D flow paths.

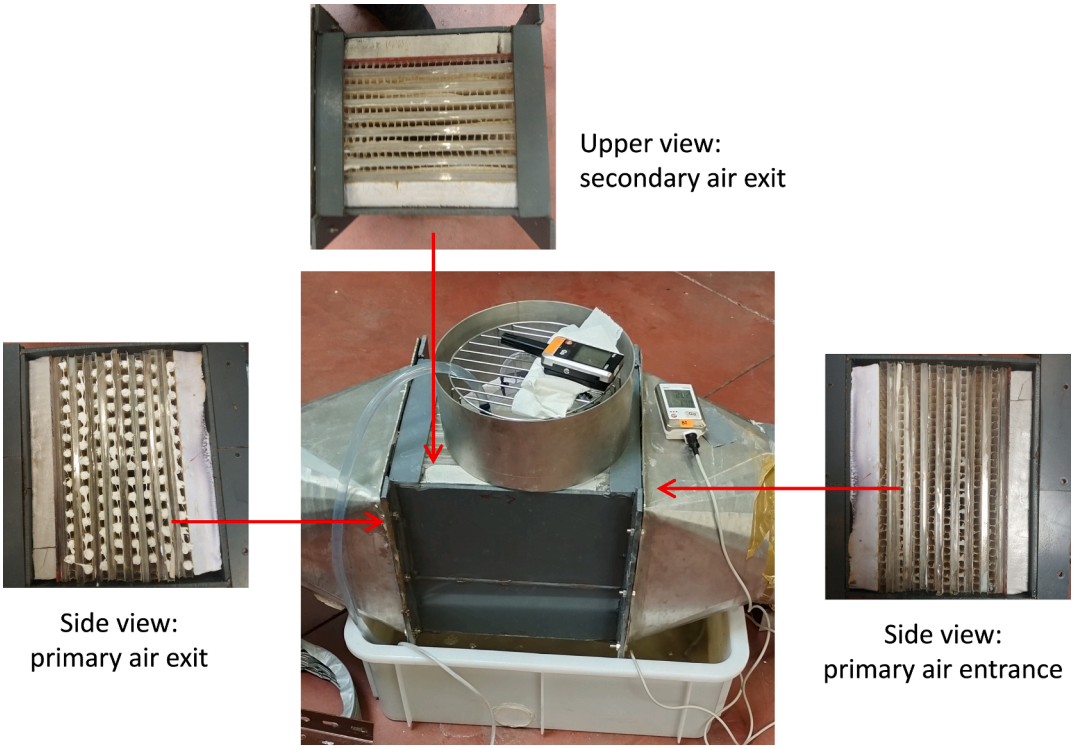

Fig. 3. Photograph of prototype. elements assembled.

(corresponding to 120 measurements) since the activation of the AHU to guarantee a constant air temperature.

Furthermore, to avoid modification of the flux line next to the orifice, the pressure was measured downstream at almost four times the diameter of the ducts.

From this point, the air volumetric flow rate $\dot{V}$ of the inlet and outlet primary air were converted to the air mass flow rates by calculating the specific volume v (Equation 2 and 3).

$$\dot{m} = \dot{V}/v \tag{2}$$

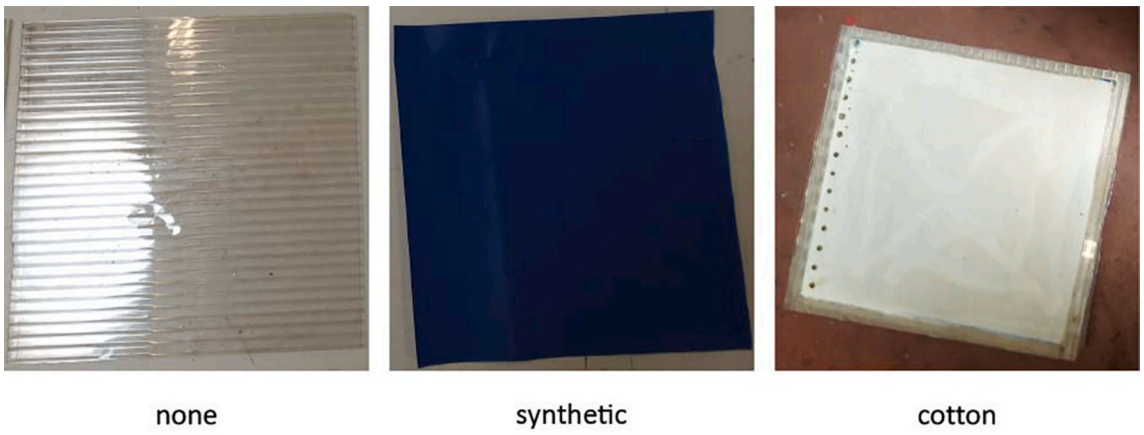

Fig. 4. View of materials tested.

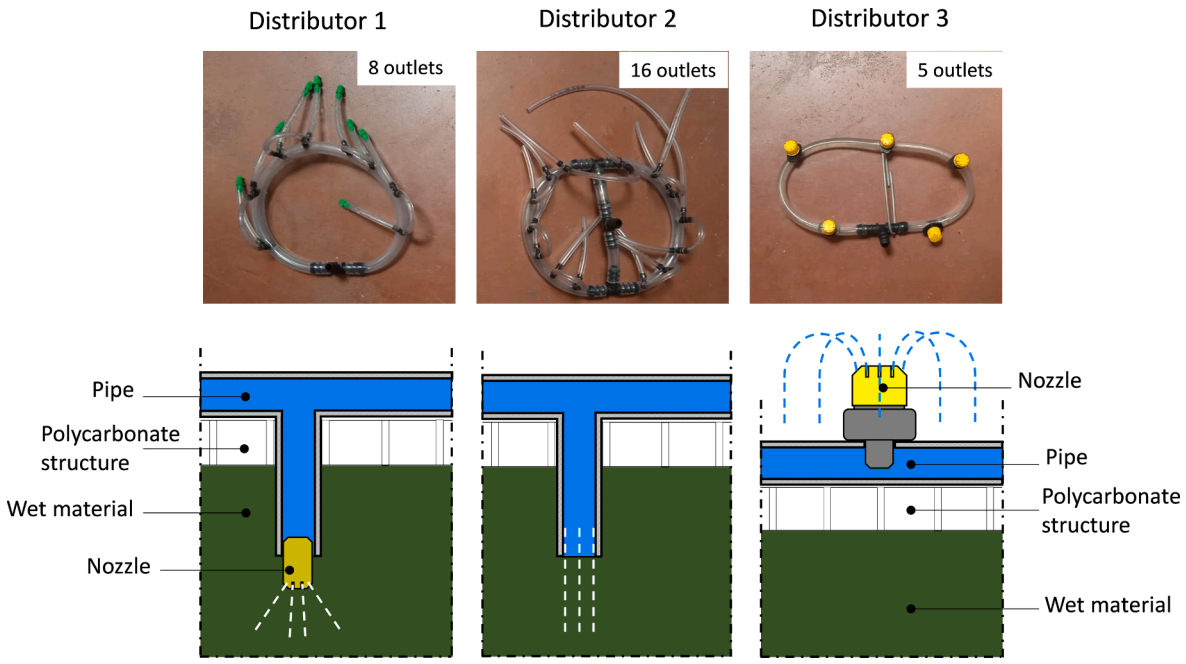

Fig. 5. Photographs and schematics of the tested water distributors.

Table 1
Description of the structural parameters of the prototype.

Parameters	Symbol	Specification/Values
Volume of Heat and Mass eXchange (HMX)		31 cm × 25 cm × 30.5 cm
Flow configuration		Mixed flow
Dry channel length	L_d	30 cm
Dry channel width	W_d	9 mm
Dry channel height	H_d	9 mm
Number of dry channels	N_d	8 x 28
Wet channel length	L_w	30 cm
Wet channel height	H_w	30 cm
Wet channel gap	G_w	9 mm
Number of wet channels	N_w	8
Plate thickness		0.5 mm
Channel material		Polycarbonate
Wicking material		None, synthetic cloth, cotton cloth
Water distributor		type 1, type 2, type 3

Specific volume v was obtained through the known psychrometric equations [38] by measuring the temperature and relative humidity for each stage and by considering the altitude (690 m.a.s.l.) of Valladolid, Spain where the laboratory is located.

Thus, by considering the mass balance in (Equation 4), the secondary air mass flow is determined (Equation 5).

$$\dot{m}_{tot} = \dot{m}_{pr} + \dot{m}_{sec} \tag{3}$$

$$\dot{m}_{sec} = \dot{m}_{tot} - \dot{m}_{pr} \tag{4}$$

Furthermore, the working-to-intake air ratio R is calculated as follows (Equation 6):

$$R = \frac{\dot{m}_{sec}}{\dot{m}_{tot}} = 1 - \frac{\dot{m}_{pr}}{\dot{m}_{tot}} \tag{5}$$

The air dry-bulb temperature and relative humidity were directly measured using the sensors described in Table 2.

These sensors were located inside the duct at the entrance of the HMX (TH-in in Fig. 6), inside the duct at the exit of the HMX (TH1-out in

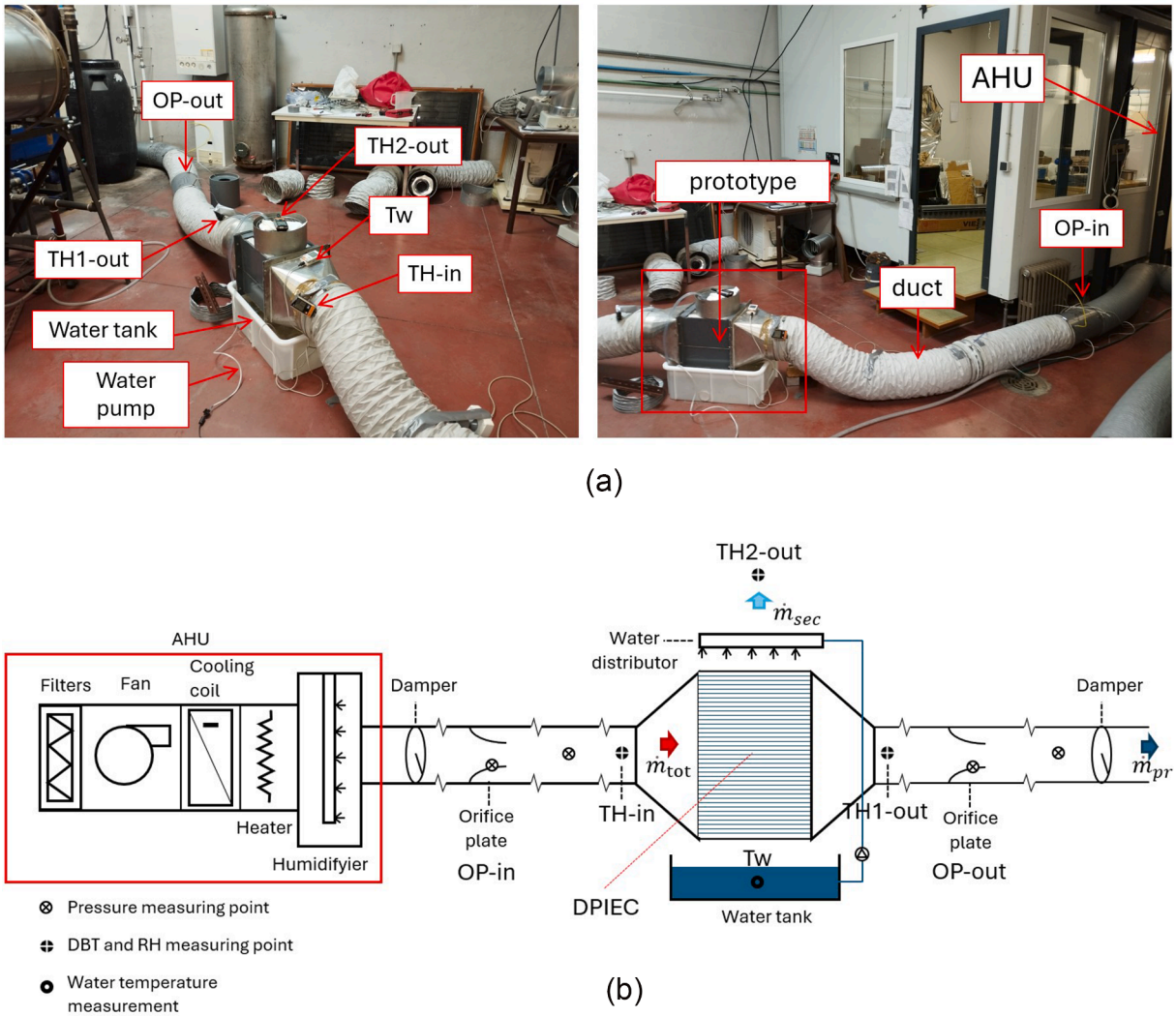

Fig. 6. Experimental set up (a) photograph and (b) scheme.

Table 2
Description of sensors (accuracy, model, measured parameters).

Parameter	Instrument	Range	Accuracy
Static pressure	Data logger Testo 435–4	0–25 hPa	±0.02 hPa (0–2 hPa) ±1% of measured values (remaining range)
Air dry bulb temperature	Testo 175 H1 Temperature and relative humidity sensor	−20–+55 °C	±0.4 °C
Air relative humidity	Testo 175 H1 Temperature and relative humidity sensor	0 %–100 %	±2% RH (from 2 %–98 % RH) at + 25 °C
Water temperature	Testo 175 T2 Temperature sensor	−35–+55 °C	±0.5 °C

Fig. 6), and at the top of the HMX at the exhaust (TH2-out in Fig. 6), respectively. The measurements were recorded every 10 s during the experiment. The water temperature was directly measured using a sensor (Tw in Fig. 6) installed inside the water tank.

2.3. Testing of the prototype

The prototype was tested by varying the wicking material and the water distributor, under different inlet air temperature conditions,

Table 3
Description of the operative conditions in each experimental test.

Test	Wicking material	Water distributor	T_{tot}	RH_{tot}	$\dot{m}_{tot}$	R
Material	Cotton cloth None Synthetic cloth	Type 3	30, 35 °C	No control 17–46 %	389 ± 11 kg/h	0.5
Distributor	Cotton cloth	Type 1 Type 2 Type 3	30, 35, 40 °C	HR control 50 % No control 26–49 %	367 ± 11 kg/h	0.5
Operative conditions	Cotton cloth	Type 3	Ambient, 30, 35, 40 °C	25–48 %	394 ± 17 kg/h	0.4–0.8

without humidity control. Further, some experiments were repeated by setting the relative humidity at 50 %. Further experiments were performed to evaluate the effect of the operative conditions.

Table 3 lists the experiments performed and the respective operative conditions.

2.4. Performance evaluation

To evaluate the performance of the DPIEC and compare it with published data, the temperature drop, effectiveness, and cooling capacity were calculated based on the experimental values.

In particular, the temperature drop is defined as the difference between total air temperature T_{tot} and primary air temperature T_{pr}.

$$\Delta T = T_{tot} - T_{pr} \tag{6}$$

Regarding the effectiveness, three different definitions were considered. In all cases, the temperature drop was compared to a maximum depression, which is representative of an ideal condition.

Therefore, by considering the wet-bulb depression in the primary channel (Equation 7) as the ideal temperature drop, wet-bulb effectiveness ε_{wb} is expressed as Equation 8.

$$WBD_{pr} = T_{tot} - WBT_{tot} \tag{7}$$

$$\varepsilon_{wb} = \frac{\Delta T}{WBD_{pr}} \tag{8}$$

where WBT_{tot} is the wet-bulb temperature of the total air mass.

By considering the dew-point depression (Equation 9) as the ideal temperature drop, dew-point effectiveness ε_{dp} is expressed as Equation 10.

$$DPD_{pr} = T_{tot} - DPT_{tot} \tag{9}$$

$$\varepsilon_{dp} = \frac{\Delta T}{DPD_{pr}} \tag{10}$$

where DPT_{tot} is the dew-point temperature of the total air mass, which is the same as that of the secondary air under the hypothesis of no mass exchange between the primary and secondary channels.

Finally, by considering the wet-bulb depression in the secondary channel (Equation 11), a second wet bulb effectiveness ε_{wb}' is expressed as Equation 12.

$$WBD_{sec} = T_{tot} - WBT_{sec,in} = T_{tot} - WBT_{pr} \tag{11}$$

$$\varepsilon_{wb}' = \frac{\Delta T}{WBD_{sec}} \tag{12}$$

where $WBT_{sec,in}$ is the wet-bulb temperature of the air at the entrance of the secondary channel, which is the same as that of primary air WBT_{pr}.

Hence, the cooling capacity is calculated by Equation 13.

$$\dot{q} = \dot{m}_{pr}(c_a + x_{in}c_v)(T_{tot} - T_{pr}) \tag{13}$$

where $\dot{m}_{pr}$ is the primary air flow rate, x_{in} is the inlet air humidity ratio, and c_{ma} is the specific heat of moist air, which is expressed by Equation (14).

$$c_{ma} = (c_a + x_{in}c_v) \tag{14}$$

where c_a and c_v are the specific heat values of the dry air and vapor, respectively.

2.5. Uncertainty analysis

Uncertainties in the values of the studied parameters were determined through the root sum squared method [39].

For the temperature drop, because the same type of sensor was used for both temperature measurements:

$$u_{\Delta T} = \sqrt{\left(\frac{\partial \Delta T}{\partial T_{tot}}u_T\right)^2 + \left(\frac{\partial \Delta T}{\partial T_{pr}}u_T\right)^2} \tag{15}$$

where the uncertainty of the measuring equipment (u_T) corresponds to the accuracy of the calibrated sensor. As indicated in Table 2, the accuracy of the temperature sensor was ± 0.4 °C, and accuracy of the temperature measurement was improved by calibrating it to u_T = 0.2 °C. Thus, the uncertainty in the temperature drop became 0.28 °C.

For the cooling capacity ($\dot{q}$), because the inlet humidity ratio in the primary airstream was maintained at a constant value, the specific heat of the moist air can be considered a constant. Having the primary air mass flow calculated by Equations (1) and (2), the uncertainty of the cooling capacity is

$$u_q = \sqrt{\left(\frac{\partial q}{\partial \Delta P}u_{\Delta P}\right)^2 + \left(\frac{\partial q}{\partial T_{tot}}u_T\right)^2 + \left(\frac{\partial q}{\partial T_{pr}}u_T\right)^2} \tag{16}$$

Since $\frac{\partial q}{\partial T_{tot}}$ and $\frac{\partial q}{\partial \Delta P}$ are increasing functions, but $\frac{\partial q}{\partial T_{pr}}$ is a decreasing function, the maximum uncertainty must be calculated in terms of the maximum values of ΔP and T_{tot}, but minimum T_{pr}.

Given the uncertainty of the instrumentation (u_T = 0.2°C, $u_{\Delta P}$ = 2 Pa), the uncertainty of the cooling capacity resulted in 24 W.

Considering the psychrometric equations required to obtain the dew-point temperature of inlet (total) air [38], the uncertainty of dew-point effectiveness:

$$u_{\varepsilon_{DP}} = \sqrt{\left(\frac{\partial \varepsilon_{DP}}{\partial HR}u_{HR}\right)^2 + \left(\frac{\partial \varepsilon_{DP}}{\partial T_{tot}}u_T\right)^2 + \left(\frac{\partial \varepsilon_{DP}}{\partial T_{pr}}u_T\right)^2} \tag{17}$$

For the uncertainty introduced by the accuracy of the instrumentation (u_T = 0.2°C, u_{HR} = 0,02), the uncertainty of dew-point effectiveness is 0.06.

Finally, the root sum squared method cannot be applied to formulate the wet-bulb effectiveness, given the iterative calculation of the wet-bulb temperature. Therefore, uncertainty was estimated as the maximum difference between the values obtained from the measurements and those achievable within the limits of accuracy of the measuring equipment (u_T = 0.2°C, u_{HR} = 0,02). The results show that the calculated values were always conservative and differed by less than 0.06.

3. Results and discussion

3.1. Test results

As an example of the experimental procedure and data logging, Fig. 7 presents the temperatures and relative humidities registered during one test. The test conditions were: air flow rate = 350–391 kg/h; working-to-intakeair ratio of 0.5; and primary air inlet temperatures = 25, 30, 35 °C, and 40 °C under uncontrolled humidity conditions and 35, 30, and 25 °C under relative humidity of 50 %. Steady-state operating conditions were identified, and the average values were determined to calculate the performance of the system.

3.2. Selection of the optimal wicking material and water distributor

This section describes the results of the experiments performed to determine the optimal wicking material and water distributor.

In particular, the wicking material was investigated by considering the device with Distributor 3. The test was repeated for the inlet temperature range of 30–35 °C without RH control. Therefore, based on thermal-hygrometric conditions of the laboratory, the relative humidity

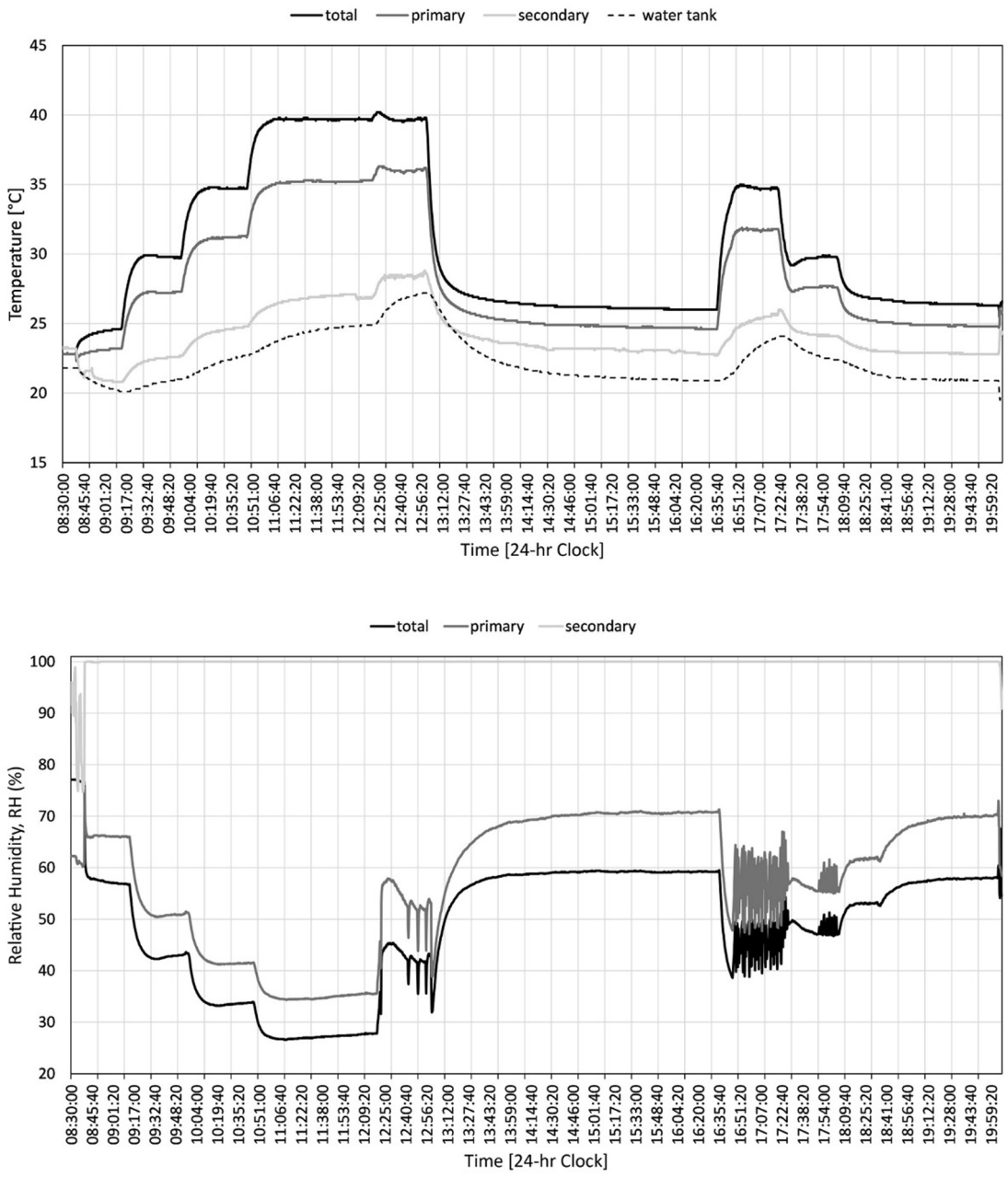

Fig. 7. Example of registered data during a test.

Table 4
Cooling capacity of different wicking materials.

Inlet air temperature (°C)	Cooling capacity (W)		
	No wicking material	**Synthetic cloth**	**Cotton cloth**
30	122.8	156.5	166.8
35	157.0	203.5	227.0

of the inlet air ranged from 17 %–46 %. The inlet mass air flow rate was 389 ± 11 kg/h, and the working-to-intake air ratio was approximately 0.5 for each test (Table 3).

Table 4 lists the cooling capacities achieved by the tested device as a function of the inlet air temperature.

The results in the table confirm that the presence of a cloth on the surface of the wet channels improves the performance of the prototype. This could be expected for the enhanced water distribution over the working area. However, the material of the fabric does not significantly influence the result. Compared to the case the wicking material, wicking by the synthetic cloth improves the cooling capacity by 27 % and 30 % at 30 and 35 °C, respectively. Meanwhile, wicking by the cotton cloth improves it by slightly higher margins (36 % and 45 %, respectively). Without the wicking material, the achievable temperature drop and wet-bulb effectiveness decrease by 0.9 °C and 0.09 at the inlet air temperature of 35 °C, respectively.

Because the difference in cooling capacity between the wicking material types is lower than its accuracy, the use of cotton cloth over synthetic cloth cannot be justified in terms of the improvement it offers. Consequently, the selection of the type of wicking material should be evaluated in relation to its cost, availability, and maintenance. However, it is worth noting that these cloths are easily accessible in the market or available as reused material; however, the possible decay of natural fibres must be also considered. In the following experiments, cotton cloth

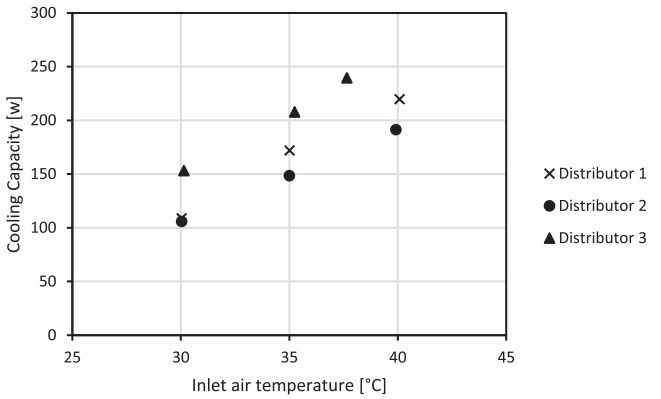

Fig. 8. Cooling capacity achieved with different water distributors (base humidity case).

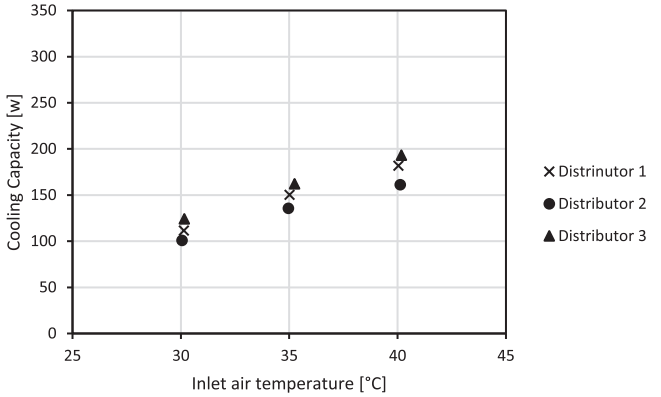

Fig. 9. Cooling capacity achieved with different water distributors (high humidity case).

is used as the wicking material.

The influence of water distributor on the device performance is investigated with the cotton cloth with and without humidity control. Tests were performed with the inlet temperatures of 30, 35, and 40 °C. The relative humidity of the inlet air without humidity control was below 50 %. The inlet mass air flow was 367 ± 11 kg/h, which corresponds to the maximum opening of the dumpers, and the working-to-intake air ratio was approximately 0.5 (Table 3).

The graphs in Fig. 8 and Fig. 9 illustrate the cooling capacity as a function of the inlet air temperature in the test without and with vapor injection in the AHU, respectively, to reproduce two levels of humidity in the inlet of the primary air, namely “base humidity” and “high humidity.”.

Distributor 3, which is composed of nozzles that uniformly spray water in the upper surface of the device (Fig. 5), performs better than Distributors 1 and 2. The worst distributor was Distributor 2, which directly distributes water inside the wet channels through small pipes (Fig. 5). This means that Distributor 3 can guarantee better saturation of the working air, despite possessing fewer outlets. Furthermore, it did not pierce in the air passage preventing channel blockage [24].

Using Distributor 3 instead of Distributor 2 can increase the achievable temperature drop and cooling capacity by up to 1.1 °C and 98.6 W, respectively, under base humidity conditions. When working under high humidity conditions, Distributor 3 increases the temperature drop by 1.0 °C and the cooling capacity by 31.9 W compared to distributor 2.

Consequently, to improve the performance of the system, Distributor 3 is selected for the following experiments.

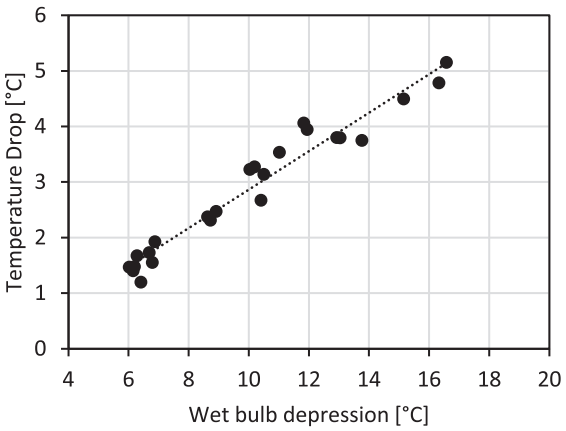

Fig. 10. Effect of wet-bulb depression (WBD) on the temperature drop.

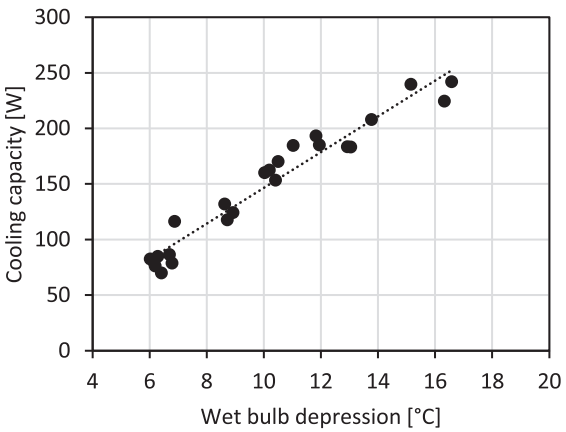

Fig. 11. Effect of WBD on the cooling capacity.

3.3. Performance evaluation

3.3.1. Effect of the inlet air conditions

This section presents the results of the experiments performed by considering the device with cotton cloth and Distributor 3 and varying the inlet air temperature and relative humidity. In particular, the inlet air temperature ranged from 23–40 °C, the relative humidity ranged from 25 %–50 %, the air mass flow air was 394 ± 17 Kg/h, and the working-to-intake air ratio approximately 0.5 (Table 3).

Results of the temperature drop (Fig. 10) and cooling capacity (Fig. 11) are represented in terms of the WBD in the primary channel, to evaluate the effects of the inlet air temperature and humidity.

Fig. 10 and Fig. 11 reveal that the temperature drop, as well as the cooling capacity, increases linearly with the WBD. This clearly demonstrates that the device performs better for the intake air with higher temperatures and lower humidities, owing to the larger potential of the evaporative cooling effect. Furthermore, this implies that the ratio between the temperature drop and the WBD, namely the wet-bulb effectiveness, could be considered a constant. In other words, the wet-bulb effectiveness does not depend on the intake air conditions.

Table 5
Average and standard deviations of wet-bulb and dew-point effectiveness at 30, 35, and 40 °C.

Inlet air temperature (°C)	ε_{wb}	ε_{wb}'	ε_{dp}
30	0.268 ± 0.009	0.261 ± 0.026	0.189 ± 0.010
35	0.300 ± 0.022	0.283 ± 0.027	0.218 ± 0.021
40	0.320 ± 0.024	0.301 ± 0.022	0.243 ± 0.024

This result is not consistent with those reported in the literature [22]. The reason of this discrepancy could be that the temperature drop achieved by the tested device was below the values obtained in other works owing to the shorter air pathway in the wet channels [22]. Therefore, a constant value of wet-bulb effectiveness can be considered in the case of small dew-point evaporative coolers. This result may be particularly useful for simulating similar small devices because it could simplify the mathematical model.

Table 5 lists the wet-bulb effectiveness in terms of the WBD of the primary air inlet and the WBD of the secondary air inlet, along with the dew point effectiveness, at the inlet temperature conditions of 30 °C, 35 °C, 40 °C.

By considering the average values, the primary wet-bulb effectiveness ranges between 0.27 and 0.32, the secondary wet-bulb effectiveness between 0.26 and 0.30, and the dew-point effectiveness between 0.19 and 0.25. Because the differences between the values obtained at varying inlet air temperatures fall below the uncertainties of the wet-bulb and dew-point effectiveness, the effectiveness parameters can be assumed to have constant values.

The results show a minor difference in considering the primary wet-bulb effectiveness instead of the secondary. This is due to the similar WBD in the secondary channel to that of the primary channel. The discussion in terms of one or other parameter in this case is approximately the same; however, the difference would become relevant in larger devices where larger temperature drops in the primary air are expected, and consequently larger differences in the WBD of the secondary air with respect to that of the primary air.

The dew-point effectiveness follows the same trend as the wet-bulb effectiveness in the same range of inlet air temperature.

3.3.2. *Effect of the working-to-intake air ratio*

The following results refer to the experiments performed by considering the device with cotton cloth and Distributor 3 and changing the working-to-intake ratio from 0.4 to 0.8. The inlet air temperature was 30 °C, the relative humidity was between 42 % and 48 %, the air mass flow air was 375 ± 13 Kg/h.

Fig. 12 and Fig. 13 illustrate the effects of the working-to-intake air ratio on the temperature drop and cooling capacity, respectively.

The graphs show that, while the drop temperature increased by approximately 0.4 °C as the working-to-intake air ratio increased from 0.4 to 0.8, the cooling capacity decreased by approximately 56 %. As expected, a higher secondary air mass flow rate will reduce the supply air mass flow rate; hence, the cooling capacity decreases despite the higher temperature drops.

Studies [14,22] have shown that both temperature drop and cooling capacity increased for higher working-to-intake ratio up to 0.3, and subsequently decreased. Hence, this value was considered as the optimal working-to-intake ratio. Consistent with the literature, the results of this study indicate decreasing values of the cooling capacity with an increasing working-to-intake ratio in the tested range beyond the optimal value of 0.3. Thus, to improve the performance of the prototype, we recommend considering lower working-to-air ratios with respect to those used in the tested device.

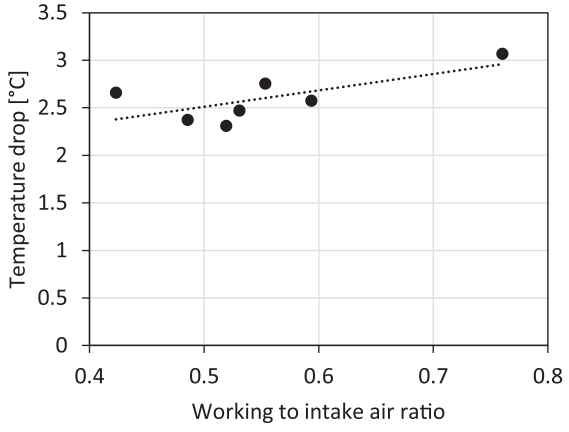

Fig. 12. Effect of the working-to-intake air ratio on temperature drop.

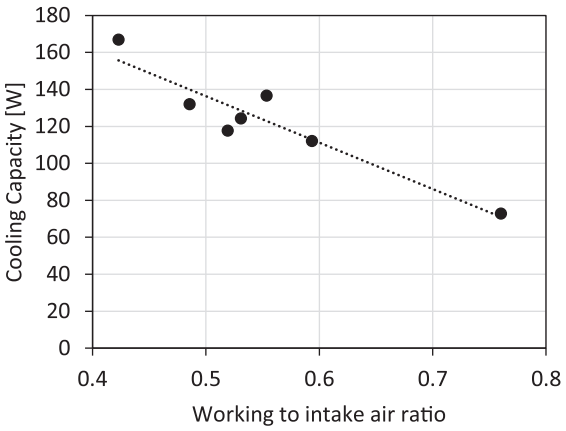

Fig. 13. Effect of the working-to-intake air ratio on cooling capacity.

3.4. *Validation against data from the literature*

Table 6 compares the performance of the prototype investigated with other the results of studies in the literature. To the best of the authors' knowledge, Deepak et al. [22] is the only study that examined a mixed-flow DPIEC. Therefore, we selected it for the comparative study. Reference [40] was chosen despite the different flow configuration because they used similar materials for their prototype.

The results reported in the table refer to the experiments performed with the same inlet air temperature equal to 35 °C and inlet air humidity ratio ranging from 11–13 g/kg.

In particular, the prototype in [22] was composed of 35 pairs of dry and wet channels made of Al sheets and cotton fibre inside the wet channels. The dimensions of surface between the dry and wet channels were 0.8 m x 0.4 m; hence, the entire heat transfer area was estimated to be 22.08 m^2. They achieved a temperature drop of 14 °C.

The same temperature drop was achieved in [40]. Their device was designed with the counter-flow configuration, and it was composed of five wet channels and four dry channels. The walls were made of polyurethane and covered with cotton fibre on the wet side. The dimensions of the surface between the dry and wet channels were 1.2 m x 0.8 m, with an estimated heat transfer area of 7.68 m^2.

The temperature drop achieved by the prototype investigated in this study was approximately 4 °C, which is less than the values reported in other studies. However, it concurs with previous results when divided among the respective heat transfer areas. More specifically, the investigated device decreased the inlet air temperature by 2.6 °C per unit of heat transfer area (°C/m^2), against 0.6 and 1.8 °C/m^2 compared with the devices in [22] and [40], respectively. This demonstrates the overall improved performance of the proposed compact design.

However, further factors may influence the results, such as the different values of intake air mass flow rate and working-to-intake air ratio. Therefore, the results were further validated against the data-driven model by [16], as reported in Table 7.

The model can calculate the temperature drop using the known inlet air temperature T_{IN}, relative humidity HR_{in}, and velocity v_{in}, length L_D and height h_{dry} of the dry channels, and working-to-intake air ratio η. The model provides two different calculations depending on the counter-flow or cross-flow configuration. This means that the model is not adapted for the mixed-flow configuration. Nevertheless, to validate

Table 6
Comparison of results with those of experimental studies in the literature at inlet DBT of 35 °C and humidity ratio of 11–13 g/kg.

Reference	Flow configuration	Plate/Wicking material	A_{HT} [m^2]	$\dot{m}$[kg/s]	v [m/s]	R [-]	ΔT [°C]	ΔT/ A_{HT} [°C/ m^2]
Current study	Mixed	Polycarbonate/ Cotton	1.44	0.1	5	0.5	3.8	2.6
Deepak et al. 2022 [22]	Mixed	Al/ Cotton	22.08	0.2	–	0.3	14	0.6
Riangvilaikul and Kumar, 2009 [40]	Counter	Polyurethane/ Cotton	7.68	–	2.4	0.3	14	1.8

Table 7
Application of the data-driven model by Sohani et al. [16] to the current experimental work.

Experimental data							Data-driven model		
T_{in} [°C]	HR_{in} [%]	V_{in} [m/s]	L_{dry} [cm]	h_{dry} [cm]	R [-]	ΔT [°C]	ΔT_{CoF} [°C]	ΔT_{CrF} [°C]	$\Delta T_{Mix\ Flow}$ [°C]
35	33	5	30	0.8	0.5	3.78	2.16	5.78	3.97

the results, the average value of temperature drops of both configurations is provided in Table 7. The results show that applying the data-driven model by Sohani et al [16] to the inlet experimental conditions provide similar results to the measured values.

4. Conclusions

This study developed and experimentally tested a novel mixed-flow DPIEC. The goals of the design were low production costs, low complexity of equipment, and compactness. Therefore, the device was a small prototype made of polycarbonate sheets with an overall volume of (31 x 25 x 30.5) cm^3.

The mixed-flow configuration was proposed to balance the high effectiveness of the counter-flow configuration with the ease of construction of the cross-flow configuration. Plates covered with a wicking material was selected to be consistent with the most recent developments. The novelties of the study were the polycarbonate plates and analysis of the effects of two different wicking materials.

The prototype was tested without any wicking material, with synthetic cloth, and with cotton cloth. The results revealed that the presence of a cloth on the surface of the wet channel improved the performance of the prototype by up to 1.45 times. However, the type of material did not yield any significant differences in performance. Consequently, the selection of the wicking material type was based on cost, availability, and maintenance.

Despite the effect of water distribution being generally disregarded in the literature, a few published works on the topic agreed on the importance of uniform water distribution. The developed prototype is thus characterized with three different water distributors. The results demonstrated that the use of nozzles that spray the water uniformly over the upper surface of the device achieved a greater temperature drop of 1 °C and approximately 100 W higher cooling capacity than the ones that penetrate the wet side of the heat exchanger, despite possessing fewer outlets.

Furthermore, the effects of the wet-bulb depression and working-to-intake air ratio were observed. By considering the best design option (cotton cloth as the wicking material and water distributor with external nozzles), the temperature drop ranged between 1 and 5 °C and the cooling capacity between 100 and 250 W, depending on the wet-bulb depression. The wet-bulb effectiveness was approximately constant, and its average value was 0.3 when the inlet air temperature was 35 °C. The average value of the dew-point effectiveness under the same inlet air conditions was 0.2.

Regarding the effect of the working-to-intake air ratio, the results showed that the temperature drop increased by approximately 33 % in the range of 0.4–0.8. However, the cooling capacity decreased by approximately 56 %. Thus, we recommend considering lower working-to-intake air ratios with respect to those used in the tested device, according to the optimal values suggested in extant literature.

Finally, the results are consistent with those of previous studies. The smaller temperature drop compared with those of other prototypes is attributed to the smaller dimensions of the prototype. However, the current prototype decreased the inlet air temperature by 2.63 °C per unit of heat transfer area against 0.63 °C/m^2 and 1.82 °C/m^2 compared with similar configurations studied in the literature. This compactness of the device could make it more attractive for commercialization.

These results should guide future DPIEC designs in terms of flow configuration, wicking selection, and water distribution design.

Declaration of competing interest

The authors declare that they have no known competing financial interests or personal relationships that could have appeared to influence the work reported in this paper.

Data availability

Data will be made available on request.

Acknowledgements

This work was developed within the research project TED2021-129652A-C22, funded by MCIN/AEI/10.13039/501100011033 and the European Union through the “NextGenerationEU”/PRTR.

Appendix A. Supplementary material

Supplementary data to this article can be found online at https://doi.org/10.1016/j.applthermaleng.2024.124294.

References

[1] U. Dubois, A. Sinea, Methodological Challenges in Energy Poverty Research, Int. J. Mark. Res. 65 (2023) 340–358, https://doi.org/10.1177/14707853231155393.
[2] H. Thomson, N. Simcock, S. Bouzarovski, S. Petrova, Energy poverty and indoor cooling: An overlooked issue in Europe, Energy Build 196 (2019) 21–29, https://doi.org/10.1016/j.enbuild.2019.05.014.
[3] EEA, Cooling buildings sustainably in Europe: exploring the links between climate change mitigation and adaptation, and their social impacts, 2022.
[4] Z. Duan, C. Zhan, X. Zhang, M. Mustafa, X. Zhao, B. Alimohammadisagvand, A. Hasan, Indirect evaporative cooling: Past, present and future potentials, Renew. Sustain. Energy Rev. 16 (2012) 6823–6850, https://doi.org/10.1016/j.rser.2012.07.007.
[5] S. Pezzutto, G. Quaglini, P. Riviere, L. Kranzl, A. Novelli, A. Zambito, E. Wilczynski, Screening of Cooling Technologies in Europe: Alternatives to Vapour Compression and Possible Market Developments, Sustainability (switzerland) 14 (2022), https://doi.org/10.3390/su14052971.

[6] S. Abdullah, M.N.B.M. Zubir, M.R. Bin Muhamad, K.M.S. Newaz, H.F. Öztop, M. S. Alam, K. Shaikh, Technological development of evaporative cooling systems and its integration with air dehumidification processes: A review, Energy Build. 283 (2023), https://doi.org/10.1016/j.enbuild.2023.112805.
[7] P. Xu, X. Ma, X. Zhao, K.S. Fancey, Experimental investigation on performance of fabrics for indirect evaporative cooling applications, Build Environ. 110 (2016) 104–114, https://doi.org/10.1016/j.buildenv.2016.10.003.
[8] H.E. Beck, N.E. Zimmermann, T.R. McVicar, N. Vergopolan, A. Berg, E.F. Wood, Cooling buildings sustainably in Europe: exploring the links between climate change mitigation and adaptation, and their social impacts, Nature Scientific Data (2018).
[9] J.R. Watt, Evaporative Air Conditioning Handbook, 1st ed., Springer, New York, NY, 2011.
[10] A. Tejero-González, A. Franco-Salas, Direct evaporative cooling from wetted surfaces: Challenges for a clean air conditioning solution, Wiley Interdiscip. Rev. Energy Environ. 11 (2022), https://doi.org/10.1002/wene.423.
[11] ASHRAE, Evaporative cooling, in: ASHRAE Handbook HVAC Applications, 2023.
[12] L. Lai, X. Wang, E. Hu, K. Choon Ng, A vision of dew point evaporative cooling: opportunities and challenges, Appl. Therm. Eng. 244 (2024) 122683, https://doi.org/10.1016/j.applthermaleng.2024.122683.
[13] M.H. Mahmood, M. Sultan, T. Miyazaki, S. Koyama, V.S. Maisotsenko, Overview of the Maisotsenko cycle – A way towards dew point evaporative cooling, Renew. Sustain. Energy Rev. 66 (2016) 537–555, https://doi.org/10.1016/j.rser.2016.08.022.
[14] C. Zhan, Z. Duan, X. Zhao, S. Smith, H. Jin, S. Riffat, Comparative study of the performance of the M-cycle counter-flow and cross-flow heat exchangers for indirect evaporative cooling - Paving the path toward sustainable cooling of buildings, Energy 36 (2011) 6790–6805, https://doi.org/10.1016/j.energy.2011.10.019.
[15] L. Jie, K.J. Chua, Indirect Dew-Point Evaporative Cooling: Principles and Applications, Springer, 2023.
[16] A. Sohani, H. Sayyaadi, N. Mohammadhosseini, Comparative study of the conventional types of heat and mass exchangers to achieve the best design of dew point evaporative coolers at diverse climatic conditions, Energy Convers. Manag. 158 (2018) 327–345, https://doi.org/10.1016/j.enconman.2017.12.042.
[17] R. Kousar, M. Ali, M.K. Amjad, W. Ahmad, Energy, Exergy, Economic, Environmental (4Es) comparative performance evaluation of dewpoint evaporative cooler configurations, J. Build. Eng. 45 (2022), https://doi.org/10.1016/j.jobe.2021.103466.
[18] G. Zhu, T. Wen, Q. Wang, X. Xu, A review of dew-point evaporative cooling: Recent advances and future development, Appl. Energy 312 (2022), https://doi.org/10.1016/j.apenergy.2022.118785.
[19] A. Pacak, K. Sierpowski, B. Baran, Z. Malecha, W. Worek, S. Cetin, D. Pandelidis, Impact of air distribution on dew point evaporative cooler thermal performance, Appl Therm Eng 224 (2023), https://doi.org/10.1016/j.applthermaleng.2023.120137.
[20] L. Jia, J. Liu, C. Wang, X. Cao, Z. Zhang, Study of the thermal performance of a novel dew point evaporative cooler, Appl. Therm. Eng. 160 (2019), https://doi.org/10.1016/j.applthermaleng.2019.114069.
[21] A.F. Boudjabi, C. Maalouf, T. Moussa, D. Abada, D. Rouag, M. Lachi, G. Polidori, Analysis and multi-response optimization of two dew point cooler configurations using the desirability function approach, Energy Rep. 7 (2021) 5289–5304, https://doi.org/10.1016/j.egyr.2021.08.128.
[22] C. Deepak, R. Naik, S.C. Godi, C.K. Mangrulkar, P. H.K., Thermal performance analysis of a mixed-flow indirect evaporative cooler, Appl. Therm. Eng. 217 (2022). https://doi.org/10.1016/j.applthermaleng.2022.119155.
[23] B.C. Wang, M. Garcia, C.D. Wei, G.G. Cheng, W. Pang, T. Bui, Development and performance analysis of a compact counterflow dew-point cooler for tropics, Therm. Sci. Eng. Prog. 46 (2023), https://doi.org/10.1016/j.tsep.2023.102218.
[24] M. Zhu, J. Lv, B. Zhou, W. Xi, L. Wang, E. Hu, Study on the performance of a novel dew-point evaporative cooler based on fiber membrane automatic wicking, Sci. Technol. Built. Environ. 29 (2023) 574–587, https://doi.org/10.1080/23744731.2023.2194194.
[25] D. Pescod, An evaporative air cooler using a plate heat exchanger , 1974.
[26] F. Comino, M.J. Romero-Lara, M. Ruiz de Adana, Experimental and numerical study of dew-point indirect evaporative coolers to optimize performance and design, Int. J. Refrig 142 (2022) 92–102, https://doi.org/10.1016/j.ijrefrig.2022.06.006.
[27] J. Lv, H. Xu, T. Xu, H. Liu, J. Qin, Study on the performance of a unit dew-point evaporative cooler with fibrous membrane and its application in typical regions, Case Stud. Therm. Eng. 24 (2021), https://doi.org/10.1016/j.csite.2021.100881.
[28] S. Alfraidi, A. Mesloub, M. Alshenaifi, E. Noaime, A. Ahriz, R. Boukhanouf, Experimental investigation of thermal performance of three configurations evaporative cooling systems (ECS) using synthetic grass wet media materials, Energy Build 306 (2024), https://doi.org/10.1016/j.enbuild.2024.113956.
[29] J. Lv, H. Xu, M. Zhu, Y. Dai, H. Liu, Z. Li, The performance and model of porous materials in the indirect evaporative cooling system: A review, J. Build. Eng. 41 (2021), https://doi.org/10.1016/j.jobe.2021.102741.
[30] J. Chu, W. Xu, Y. Fu, H. Huo, Experimental research on the cooling performance of a new regenerative dew point indirect evaporative cooler, J. Build. Eng. 43 (2021), https://doi.org/10.1016/j.jobe.2021.102921.
[31] S. De Antonellis, C.M. Joppolo, P. Liberati, S. Milani, F. Romano, Modeling and experimental study of an indirect evaporative cooler, Energy Build 142 (2017) 147–157, https://doi.org/10.1016/j.enbuild.2017.02.057.
[32] T. Sun, X. Huang, Y. Chen, H. Zhang, Experimental investigation of water spraying in an indirect evaporative cooler from nozzle type and spray strategy perspectives, Energy Build 214 (2020), https://doi.org/10.1016/j.enbuild.2020.109871.
[33] X. Ma, W. Shi, H. Yang, Spray parameter analysis and performance optimization of indirect evaporative cooler considering surface wettability, J. Build. Eng. 82 (2024), https://doi.org/10.1016/j.jobe.2023.108175.
[34] W. Shi, H. Yang, X. Ma, X. Liu, A novel indirect evaporative cooler with porous media under dual spraying modes: A comparative analysis from energy, exergy, and environmental perspectives, J. Build. Eng. 76 (2023), https://doi.org/10.1016/j.jobe.2023.106874.
[35] P. Xu, X. Ma, X. Zhao, K. Fancey, Experimental investigation of a super performance dew point air cooler, Appl Energy 203 (2017) 761–777, https://doi.org/10.1016/j.apenergy.2017.06.095.
[36] Y. Wan, T. Xue, Z. Huang, A. Soh, H. Liu, K.J. Chua, Comparative study on performance of counter-flow dew-point indirect evaporative cooling systems via a more realistic and experimentally validated three-dimensional model, J. Build. Eng. 82 (2024), https://doi.org/10.1016/j.jobe.2023.108408.
[37] S. Kashyap, J. Sarkar, A. Kumar, Effect of surface modifications and using hybrid nanofluids on energy-exergy performance of regenerative evaporative cooler, Build. Environ. 189 (2021), https://doi.org/10.1016/j.buildenv.2020.107507.
[38] ASHRAE, Chapter 1. Psychtometrics, in: ASHRAE Handbook: Fundamentals, 2021.
[39] R.J. Moffat, Describing the Uncertainties in Experimental Results, Standford University, Stanford, California, 1988.
[40] B. Riangvilaikul, S. Kumar, An experimental study of a novel dew point evaporative cooling system, Energy Build 42 (2010) 637–644, https://doi.org/10.1016/j.enbuild.2009.10.034.